LETTER • **OPEN ACCESS**

Comparison of a simple hydrostatic and a data-intensive 3D numerical modeling method of simulating sea-level rise induced groundwater inundation for Honolulu, Hawai'i, USA

Environmental Research Communications

LETTER

Comparison of a simple hydrostatic and a data-intensive 3D numerical modeling method of simulating sea-level rise induced groundwater inundation for Honolulu, Hawai'i, USA

Shellie Habel[1], **Charles H Fletcher**[1], **Kolja Rotzoll**[2], **Aly I El-Kadi**[1,2] and **Delwyn S Oki**[3]

[1] University of Hawai'i at Mānoa, School of Ocean and Earth Science and Technology, Department of Geology and Geophysics, POST Building, Suite 701, 1680 East-West Road, Honolulu, HI 96822, United States of America
[2] University of Hawai'i at Mānoa, Water Resources Research Center, 2540 Dole St., Holmes Hall 283, Honolulu, HI 96822, United States of America
[3] USGS Pacific Islands Water Science Center, 1945 Wasp Blvd., B176, Honolulu, HI 96818, United States of America

E-mail: skey@hawaii.edu

Keywords: sea-level rise, groundwater inundation, adaptation, flood simulations, bathtub modeling

OPEN ACCESS

RECEIVED
21 January 2019

REVISED
23 March 2019

ACCEPTED FOR PUBLICATION
16 May 2019

PUBLISHED
24 May 2019

Abstract

Groundwater inundation (GWI) is a particularly challenging consequence of sea-level rise (SLR), as it progressively inundates infrastructure located above and below the ground surface. Paths of flooding by GWI differ from other types of SLR flooding (i.e., wave overwash, storm-drain backflow) such that it is more difficult to mitigate, and thus requires a separate set of highly innovative adaptation strategies to manage. To spur consideration of GWI in planning, data-intensive numerical modeling methods have been developed that produce locally specific visualizations of GWI, though the accessibility of such methods is limited by extensive data requirements. Conversely, the hydrostatic (or 'bathtub') modeling approach is widely used in adaptation planning owing to easily accessed visualizations (i.e., NOAA SLR Viewer), yet its capacity to simulate GWI has never been tested. Given the separate actions necessary to mitigate GWI relative to marine overwash, this is a significant gap. Here we compare a simple hydrostatic modeling method with a more deterministic, dynamic and robust 3D numerical modeling approach to explore the effectiveness of the hydrostatic method in simulating equilibrium aquifer effects of multi-decadal sea-level rise, and in turn GWI for Honolulu, Hawai'i. We find hydrostatic modeling in the Honolulu area and likely other settings may yield similar results to numerical modeling when referencing the local mean higher-high water tide datum (generally typical of flood studies). These findings have the potential to spur preliminary understanding of GWI impacts in municipalities that lack the required data to conduct rigorous groundwater-modeling investigations. We note that the methods explored here for Honolulu do not simulate dynamic coastal processes (i.e., coastal erosion, sediment accretion or changes in land cover) and thus are most appropriately applied to regions that host heavily armored shorelines behind which GWI can develop.

1. Introduction

Sea-level rise (SLR) presents inevitable challenges for low-lying coastal municipalities (Hallegatte *et al* 2013, Hinkel *et al* 2014). Even as SLR projections evolve, many researchers have concluded that flooding will grow progressively damaging within decades (Kulp and Strauss 2017, Sweet *et al* 2018). This is especially true for regions where rates of SLR exceed the global mean (i.e., East and Gulf Coasts of the US) (Sweet *et al* 2017). High-tide flooding is already problematic at these locations resulting in drainage failure, road closure, and the deterioration of municipal infrastructure (Sweet and Park 2014).

To avoid overwhelming losses from flooding and infrastructure failure, adaptive-management consideration ideally would be given to SLR flood scenarios in municipal planning, policy writing, and project implementation (de Moel *et al* 2014, Hinkel *et al* 2014). This is progressing in several municipalities where locally pertinent SLR flood maps guide planning decisions (The New York State Sea Level Rise Task Force 2010, Mitchell *et al* 2013, Horton *et al* 2015, Climate Ready Boston 2016, Office of Resilience, Department of Regulatory and Economic Resources, Miami-Dade County, Florida 2016, Rutgers University NJADAPT (2017), Hawai'i Climate Change Mitigation and Adaptation Commission (2017)). However, assessment has not progressed in regions lacking the necessary resources to produce such maps, even where similar vulnerabilities to SLR exist. Moreover, the absence of flood simulations has been cited as one of the main impediments to adaptation planning and policy development (Bierbaum *et al* 2013).

Groundwater inundation (GWI) has been identified as one of the more problematic components of SLR flooding, because the water table can evade coastal barriers designed to mitigate surface-water inundation as it is lifted through the ground surface (Rotzoll and Fletcher 2013). Damage to municipal infrastructure will ensue as groundwater rises above critical elevation thresholds; first somewhat discreetly as buried assets become submerged, and then more obviously as groundwater breaches the ground surface (Habel *et al* 2017). The GWI component of flooding will occur contemporaneous with, and in some cases ahead of, non-storm marine components (i.e., wave overwash, storm-drain backflow) and will require a separate set of planning and engineering efforts to manage (Habel *et al* 2017). Despite the expected significance of GWI in SLR flooding, GWI has not been widely recognized as a critical element of long-range planning.

Studies undertaken in Honolulu, Hawai'i have been among the first to specifically simulate the GWI component of SLR flooding, using 1D analytical (Rotzoll and Fletcher 2013) and 3D numerical (Habel *et al* 2017) methods. These methods use the diffusion equation to simulate groundwater levels in the coastal zone, and further determine where GWI is likely to develop by identifying locations where surface topography will fail to accommodate SLR induced increases in water-table height.

GWI has also been simulated using the hydrostatic method, also known as the 'bathtub' or 'single-surface' approach (Cooper and Chen 2013, Cooper *et al* 2013, Kane *et al* 2015). However, this method is more commonly used to identify vulnerability to direct marine flooding by characterizing locations that lie below projected sea level in a digital elevation model, when referenced to the local mean higher-high water (MHHW) datum (Marcy *et al* 2011, Strauss *et al* 2012). Elevations are generally referenced to the MHHW datum for consideration of the average daily maximum threshold of local nearshore sea level (National Oceanic and Atmospheric Administration NOAAb 2017). Incentive for widespread use of the hydrostatic method lies in the availability of high-resolution Light Detection and Ranging (LiDAR) data (LiDAR Online 2017, National Ecological Observatory Network NEON (2017), National Oceanic and Atmospheric Administration NOAAc 2017, OpenTopography 2017, United States Geological Survey USGS EarthExplorer (2017), US Army Corps of Engineers USACE National Coastal Mapping Program NCMP (2017)). In the US, interpretive maps using LiDAR are publicly available (i.e., NOAA SLR Viewer: https://coast.noaa.gov/slr/). Use of the hydrostatic method to simulate GWI has thus far been done implicitly only; assuming locations without direct connection to the marine environment, but that nonetheless fall below a reference datum, must represent some combination of GWI and storm-drain backflow. Until now, this assumption has not been tested.

Although the hydrostatic method is favored for its simplicity, it has been criticized as potentially overestimating areal flood extent by including locations lacking direct marine connection (Poulter and Halpin 2008, Gilmer and Ferdaña 2012). Some studies consider these locations artifacts of model output, and a number of studies have taken steps to exclude them from final flood simulations (i.e., Henman and Poulter 2008, Poulter and Halpin 2008, Gesch 2009, Marcy *et al* 2011). However, available mapping tools, such as the NOAA SLR Viewer, include and identify disconnected areas to address the likelihood of flooding by flow pathways not resolved in the elevation data (i.e., under bridges or covered channels) (Marcy *et al* 2011, Strauss *et al* 2012). Although excluding disconnected areas is appropriate for cases in which marine connection is the main process of inundation related to sea-level rise, excluding these areas for cases in which groundwater inundation is important may yield biased results (Rotzoll and El-Kadi 2008, Bjerklie *et al* 2012, Habel *et al* 2017).

Here, we assess the hydrostatic method with comparisons to the more comprehensive and data-intensive 3D numerical method. We explore the effectiveness of the simple hydrostatic method in simulating GWI to determine under which conditions its use might be acceptable. Ultimately, our intent is to evaluate a cost-effective and simple method to enable improved assessment of flood impacts related to SLR among municipalities that lack the capacity to conduct rigorous groundwater-modeling investigations.

1.1. Study area

The study area is located on the southeastern coastal plain of O'ahu, Hawai'i (figure 1) encompassing the primary urban corridor of Honolulu. Groundwater here is part of a larger freshwater-lens system in which the

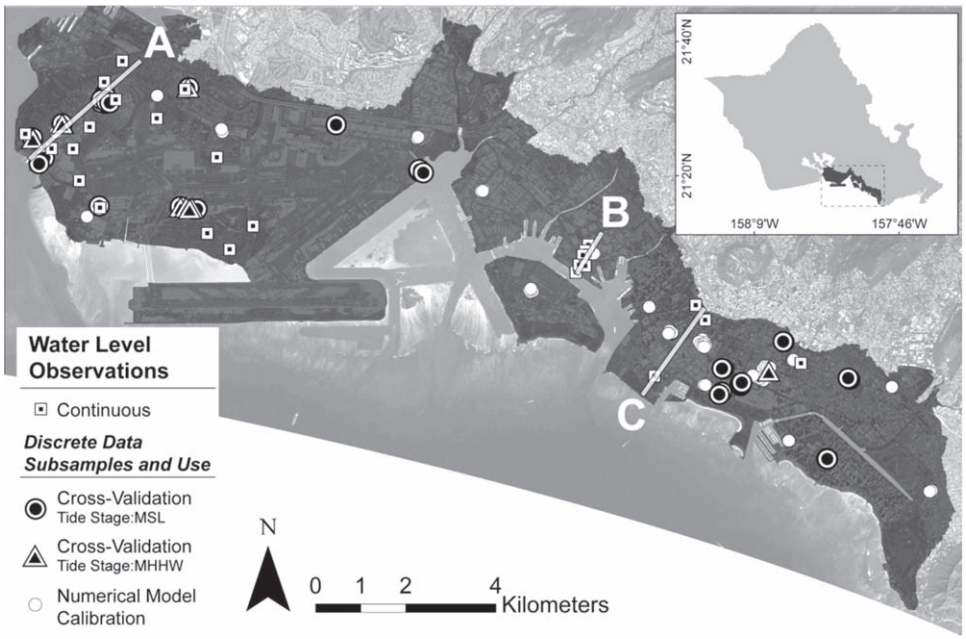

Figure 1. Primary Urban Center of Honolulu on the island of O'ahu, Hawai'i. The shaded area shows the study region including locations of water-level observations. Transects A, B, and C illustrate where groundwater-level simulations are compared in cross sections.

uppermost 100 to 200 m of the aquifer is unconfined (Macdonald *et al* 1983, Rotzoll *et al* 2010), and influenced directly by rainfall and near-shore sea-level fluctuations produced by tides, wave set-up, and longer period sea-level variations (Ponte 1994, Wu *et al* 1996, Yin *et al* 2001, Gonneea *et al* 2013, Habel *et al* 2017).

Groundwater in the unconfined aquifer is not potable owing to elevated salinity and urban contamination, and therefore is only extracted for use in small-scale irrigation and cooling towers (Whittier *et al* 2010). Flow in the unconfined aquifer is driven by the pressure gradient from the underlying confined aquifer into the unconfined aquifer, and through surficial recharge by rainfall, leakage of water-conveyance infrastructure, and small-scale irrigation (Engott *et al* 2017). The subsurface geology comprises post-erosional volcanics, alluvial debris, artificial fill, and reefal carbonates related to Quaternary sea-level high stands (Stearns and Vaksvik 1935, Ferrall 1976, Munro 1981, Finstick 1996, Izuka *et al* 2018).

1.2. Sea-level rise projections

The IPCC Fifth Assessment Report (Church *et al* 2013) estimates that global mean sea level could reach magnitudes ranging from 0.52 to 0.98 m by 2100 (relative to 1986–2005) under Representative Concentration Pathway 8.5, the 'business as usual scenario.' However, studies incorporating ice-shelf hydrofracturing and ice-cliff collapse mechanisms, triggered under high-emissions scenarios, indicate the potential for higher SLR late this century (i.e., Kopp *et al* 2017). Additionally, owing to global gravitational effects (i.e., ice fingerprinting), SLR particular to the Hawaiian Islands will likely exceed the global mean (Spada *et al* 2013, Kopp *et al* 2014, 2015). For the purpose of this comparison study, when simulating GWI, we consider a SLR magnitude of 1 m, consistent with the intermediate scenario of Sweet *et al* (2017).

2. Methods

Model accuracy is assessed by comparing simulated present-day groundwater levels produced using the hydrostatic and 3D numerical methods to groundwater-level observations compiled within the study area from monitoring wells. We consider Honolulu's mean sea-level (MSL) tide stage and MHHW tide stage (0.33 m + MSL) in model construction (National Oceanic and Atmospheric Administration NOAAa 2017).

The approach used to characterize areas vulnerable to GWI was adopted from similar studies (Rotzoll and Fletcher 2013, Cooper *et al* 2015, Habel *et al* 2017) such that GWI is characterized in locations where groundwater elevations exceed the ground-surface elevations. Ground-surface elevations were simulated using a digital elevation model (DEM) that was constructed by merging rasterized 2013 NOAA DEM tiles. The tiles were produced by NOAA using LiDAR ground-return elevation data referenced to local mean sea level (LMSL)

(National Oceanic and Atmospheric Administration NOAAb 2017). The elevation data has 0.15 m and 1 m vertical and horizontal resolution, respectively (Office for Coastal Management 2019).

2.1. Groundwater elevation data and subsets

Observations of groundwater elevations were compiled for use in 3D model calibration and to test the accuracy of model simulations. Groundwater-level data available for this study included 247 discrete water-level observations obtained from Hawai'i Department of Health Leaky Underground Storage Tank records (State of Hawaii Department of Health DOH 2018), and 73 sets of continuous water-level observations compiled from local hydrologic studies. For model calibration, 193 discrete water-level measurements were spatially subsampled and 49 continuous records were temporally subsampled from the original dataset, and the remaining measurements were used for cross-validation analysis.

Cross-validation compares simulated groundwater levels with two observation subsets representative of the MSL and MHHW scenarios. Compared to oscillations in ocean water levels, groundwater-level oscillations are attenuated, decreasing in amplitude and increasing in temporal lag as oscillations propagate inland. The influence of ocean oscillations was quantified for each set of continuous observations using the methods of Habel *et al* (2017) in which temporal lag was evaluated by cross correlating tidal signals at the Honolulu tide station with tidal signals observed in the groundwater data, and tidal efficiency was calculated using linear least-squares regression of lag-corrected groundwater time series to tidal-signal data. To accommodate the tidal-response phenomenon, data in each subset were chosen with consideration of the tidal elevation such that the tide was within 4 cm of the respective MSL or MHHW tidal scenario at the lag-corrected time of data collection. Subsamples consist of 43 discrete measurements representing the MSL scenario, 11 discrete measurements representing the MHHW scenario, and 24 continuous observations used to represent both scenarios. All discrete observations were corrected for anomalous sea-surface height using the methods of Habel *et al* (2017). The 24 continuous measurements were processed to represent MSL by calculating average recorded water levels during times with negligible rainfall and non-anomalous sea-surface levels. Measurements were processed to represent MHHW by calculating the average reconstructed tidal influence produced during the MHHW tide stage. Reconstructions of tidal influence were produced using UTIDE (Codiga 2011).

2.2. Summary of modeling methods

2.2.1. Hydrostatic model construction

In hydrostatic modeling, the groundwater hydraulic gradient and attenuated tidal response with distance inland are ignored (i.e., Marcy *et al* 2011, Strauss *et al* 2012). Thus, we set the water table to an elevation equal to simulated sea level, referenced to the MSL datum. For example, for cases in which sea level is simulated at an elevation of 0 m, the water table inland is assumed to be located at an elevation of 0 m across the entire study area. For a simulated SLR of 1 m, the water table everywhere is assumed to be at an elevation of 1 m.

2.2.2. 3D Numerical model construction

Groundwater simulation using the 3D numerical method with MODFLOW 2005 (Harbaugh 2005) follows Habel *et al* (2017), but has been extended to represent a larger study area encompassing the Primary Urban Center of Honolulu. The numerical model simulates steady-state conditions of the water table at current mean sea level and a 1-m increase in sea level. Simulated subsurface hydrogeologic conditions are based on conditions determined in regional studies (Ferrall 1976, Munro 1981, Finstick 1996, Oki 2005, Rotzoll and El-Kadi 2007). The model was calibrated using discrete and continuous water-level measurements discussed previously (figure 1).

The extended model consists of 48,483 active, 100-m uniform grid cells and three layers, representing unconsolidated caprock (model layer 1), consolidated caprock (model layer 2), and basalt (model layer 3) hydrogeological units, respectively. The inland boundary is defined by the 0 m elevation contour (figure 2) that represents the uppermost extent of the basalt aquifer (Rotzoll and El-Kadi 2007). The seaward boundary is defined by the 200-m depth contour of 2013 US Army Corps of Engineers LiDAR bathymetry data (National Oceanic and Atmospheric Administration NOAAb 2017). The top of the unconsolidated caprock unit (model layer 1) is defined by mosaicked 2013 NOAA LiDAR topography data and 2013 US Army Corps of Engineers LiDAR bathymetry data (NOAAb 2017), with a specified thickness of 10 m based on the approximate depth in which consolidated caprock material has been encountered (Ferrall 1976, Munro 1981, Finstick 1996). The consolidated caprock unit (model layer 2) extends from the base of the unconsolidated caprock unit to the uppermost extent of the basalt unit (model layer 3) as defined by elevation data that represents the uppermost extent of the basalt aquifer (Rotzoll and El-Kadi 2007). Details of the flow in the basalt aquifer unit are beyond the scope of this study. Therefore, the basalt aquifer is represented by a thin unit that extends an arbitrary 1 m

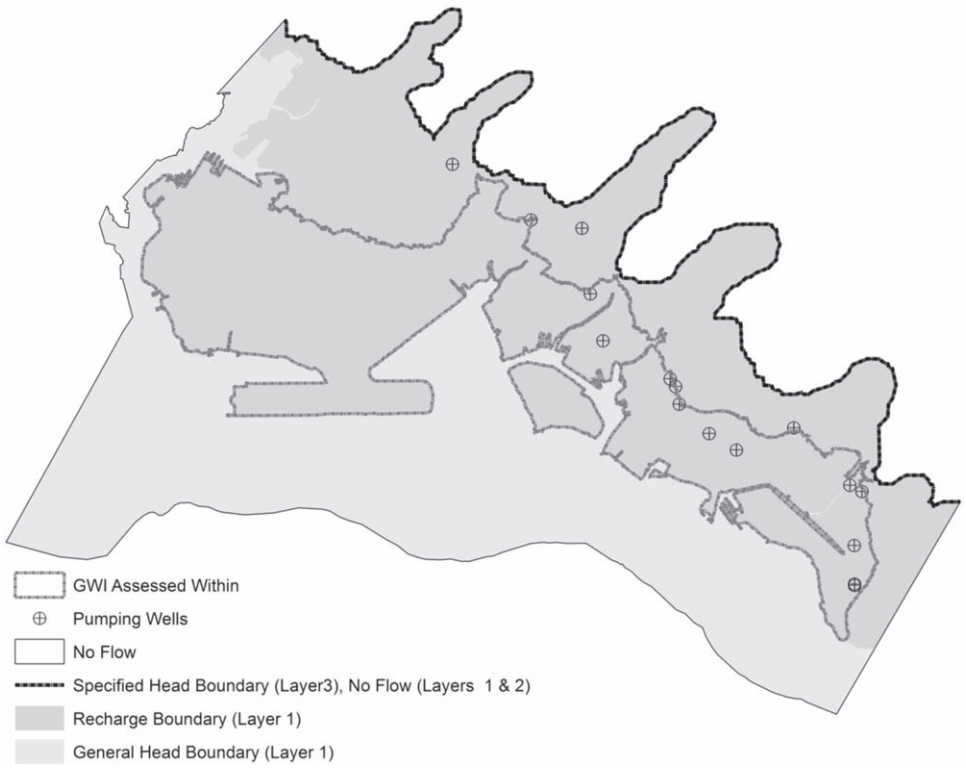

Figure 2. Diagram of model construction illustrating the application of boundary conditions. The area within which GWI was assessed is shown, and extends from the 10 m land surface elevation contour to the coastline; the area was chosen for analysis based on hosting adequate water level observations for calibration.

below the base of the consolidated caprock unit and was included exclusively to simulate flow from the basalt into the caprock aquifer in which model layers 1 and 2 represent the caprock aquifer.

The model domain is bounded on the bottom and the sides by no-flow boundaries (with the exception of the inland boundary for the bottom unit); the upper-boundary is a specified recharge boundary; the inland lateral boundary of the bottom unit (model layer 3) is a specified head boundary to simulate flow from the basalt unit to the upper caprock units (figure 2). Specified-head values were based on simulations of confined groundwater flow in southern O'ahu (Rotzoll and El-Kadi 2007). Seaward of the 0-m land-surface elevation contour, current sea-level conditions were simulated using a specified general-head boundary at the ocean bottom with a conductance of 10 m^2 d^{-1}. A 1-m increase in sea level was simulated by re-evaluating the general-head boundary seaward of the 1-m elevation contour, and by increasing the elevation of hydraulic head from 0 m to 1 m; conductance was not changed.

Well locations (figure 2) and withdrawal rates available from the State Commission on Water Resource Management were adopted from existing groundwater-flow models representative of the Honolulu aquifer (Rotzoll and El-Kadi 2007) and only those wells pumping from the caprock were considered following the application of Habel *et al* (2017). Well withdrawal rates were defined as the arithmetic mean of respective pumping rates from 1996 to 2005. Recharge data were acquired from the mean annual water-budget model for the Island of O'ahu, Hawai'i (Engott *et al* 2017), which simulated hydrological processes including rainfall, fog interception, irrigation, direct runoff, return flows from septic systems, and evapotranspiration.

Hydraulic-conductivity values for model layer 1 representing the unconsolidated caprock unit were estimated using the nonlinear inverse modeling utility, PEST in which Tikhonov preferred homogeneous regularization was used (Doherty and Hunt 2010). As part of this approach, pilot points were established on 500-m grid across the study area, totaling 361 points. All post-calibration values applied to the unconsolidated caprock unit were within the range of values previously observed for the study area, ranging from 0.001 to 854 m d^{-1} (Finstick 1996) with an average value of 135.2 m d^{-1} and standard deviation of 288.5 m d^{-1}.

Manual iterative adjustment was employed in the estimation of a hydraulic-conductivity parameter value of 1 m d^{-1} for model layer 2 representing consolidated caprock. A hydraulic conductivity of 600 m d^{-1} was specified for model layer 3 representing the basalt unit and was based on values employed in modeling studies that simulate local basalt aquifers (Rotzoll and El-Kadi 2007, Izuka *et al* 2018). A vertical anisotropy (Kh/Kv) of 3.0 was specified for all layers.

Following model calibration, the simulated mean residual water level and root-mean-squared error were 0.04 m and 0.12 m, respectively.

The specific limitations of the modeling methodology are summarized in Habel *et al* (2017) in which the main limitations include:

- The model is steady-state and thus does not assess time-dependent hydrological processes such as variations in recharge, pumping rates, boundary flows and groundwater storage, and aperiodic short-term changes in sea level by phenomena such as storm-surges, tsunamis, etc;
- MODFLOW-2005 assumes a uniform density of water, and thus does not incorporate the influence of density-driven fluid flow such as mixed seawater and freshwater flows;
- The model does not consider flow that occurs in the unsaturated zone or surface-water flow, evaporation from surface-water sources, and ponding or routing of waters that occurs once groundwater has breached the ground surface;
- The model does not consider dynamic changes in landscape (i.e., erosion) produced by SLR.

2.2.3. Tidal application

For the hydrostatic method, tidal influence was assessed by elevating the groundwater level to the tide stage elevation being simulated, thus natural attenuation of the tidal signal in an inland direction was not considered and water levels were not adjusted when simulating the MSL tide stage. As such, this method would tend to overestimate the inundation derived from groundwater when considering tides as it neglects attenuated head responses to tidal forcing.

For the 3D numerical method, tidal influence was evaluated by performing regression analyses to compute analytical solutions that assign tidal efficiency as an exponential function of distance from the coastline following the assessment in Habel *et al* (2017). Tidal efficiencies representing six subzones were calculated by comparing tidal amplitudes recorded at the NOAA Honolulu Tide station (National Oceanic and Atmospheric Administration NOAAa 2017) to those observed at continuous monitoring wells. The six subzones represent the eastern, middle, and western extent of the study area, in which the western extent was further divided into four subzones. Subdivisions were made in the western extent to represent unique patterns of observed tidal efficiencies that correlated with distinct geologic strata that constitute the shallow geology (i.e., fill, beach deposits, lagoon and reef deposits, and Honolulu Volcanics) (Sherrod *et al* 2007). Average post-calibration hydraulic conductivities within each subzone defined for the unconsolidated caprock unit are 198.6 m/d (eastern), 88.8 m d^{-1} (middle), 64.2 m d^{-1} (western-fill), 87.1 m d^{-1} (western-beach deposits), 184.7 m d^{-1} (western-lagoon and reef deposits), and 157.0 m d^{-1} (western-Honolulu Volcanics). Tidal efficiencies are expressed as increases in piezometric head considering the tidal half amplitude (h_0) as follows: $h(x)/h_0 = e^{-0.002x}$ (eastern), $h(x)/h_0 = e^{-0.005x}$ (middle), $h(x)/h_0 = 0.55e^{-0.0007x}$ (western-fill), $h(x)/h_0 = 0.43e^{-0.001x}$ (western-beach deposits), $h(x)/h_0 = 0.44e^{-0.0004x}$ (western-lagoon and reef deposits), and $h(x)/h_0 = 0.43e^{-0.0002x}$ (western-Honolulu Volcanics) in which h(x) is the increase in piezometric head (m), and x is the distance from the shoreline (m). Based on the estimated diffusivities for these units, the computed tidal efficiencies are reasonable and consistent with the hydraulic properties. Similar to Habel *et al* (2017), the analytical solutions were applied within the respective boundaries of each of the six subzones to a raster grid as a function of the distance of each grid cell to the modeled coastline. Raster values representing tidal efficiency were calculated by setting h_0 to 0.33 (the MHHW tide elevation above the MSL datum in meters), which were subsequently summed with water-table raster data from the model output to generate the tidally influenced water-table height considering the MHHW tide stage.

3. Results

3.1. Test of model

As part of cross-validation analysis, error statistics were calculated for the 3D numerical and hydrostatic methods based on the residual values between simulated and observed groundwater levels representing MSL and MHHW scenarios under current conditions (table 1).

In simulating MSL, the RMSE and systematic error (bias) of hydrostatic residuals reveal profoundly low estimates of groundwater level. This finding is reinforced by the negative maximum residual, indicating that at every comparison point, the method underestimates groundwater level. Performance improves markedly when simulating MHHW. This is evident from the significant reduction in RMSE and bias; however, the bias remains negative indicating overall underestimation of groundwater level. As expected, the RMSE representing the 3D numerical model is similar to that calculated in Habel *et al* (2017) considering both tidal scenarios.

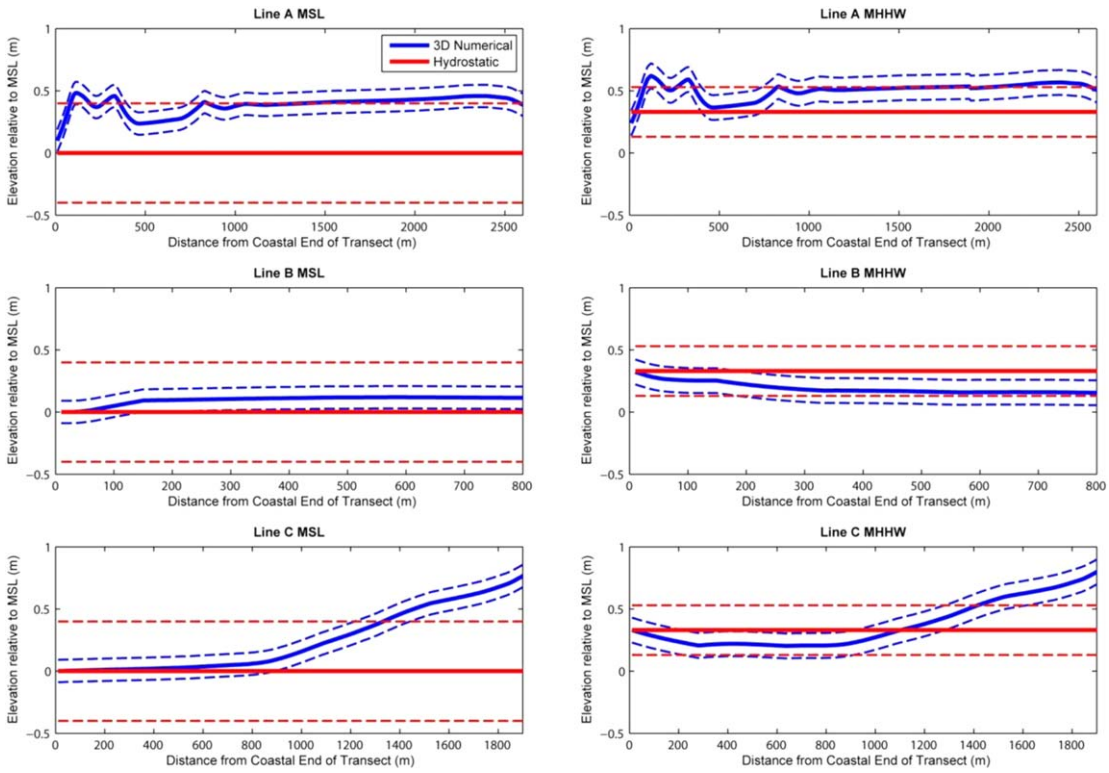

Figure 3. Composite water table simulations considering the influence of MSL (left column) and MHHW (right column) generated using hydrostatic (red) and 3D numerical (blue) simulations, along shore-normal transects (see figure 1 for location). Dotted lines denote RMSE departure from observed water levels. Lines A, B and C represent differing hydrogeologic conditions within the study area. Note that water levels along transect A dip at the inland extent due to the backshore presence of Pearl Harbor.

Table 1. Comparison of error statistics calculated for model residuals. Simulations considering MSL and MHHW scenarios are analyzed. Calculations include root mean squared error (RMSE), mean (μ), median, skew, standard deviation (σ), minimum and maximum residual values.

Tide stage: MSL Model Type	**RMSE (cm)**	**μ (cm)**	**Median (cm)**	**Skew**	**σ (cm)**	**Min (cm)**	**Max (cm)**
Hydrostatic	40	−33	−34	0.33	14	−57	−1
3D Numerical	9	−2	−3	0.05	9	-24	16
Tide stage: MHHW Model Type	**RMSE (cm)**	**μ (cm)**	**Median (cm)**	**Skew**	**σ (cm)**	**Min (cm)**	**Max (cm)**
Hydrostatic	20	−8	−7	0.15	18	−50	32
3D numerical	10	3	5	−0.44	9	−18	20

Simulated groundwater levels are illustrated in cross-section along shore-normal transects (figure 3). Cross-section locations represent regions that feature different hydraulic gradients with distinctive subsurface geologies. Transect A represents a calcium carbonate platform comprising mainly Pleistocene skeletal limestone; Transect B represents alluvium and fill; Transect C represents limestone and fill and rises relatively abruptly in elevation. Results indicate that, although the hydrostatic simulations do not thoroughly align with the more robust model, the RMSE overlaps with results of the 3D numerical simulations (other than on transect C landward of approximately 1500 m). This is true for both evaluated tide scenarios, however, for the hydrostatic simulations the RMSE of the MHHW scenario is half that of the MSL scenario.

3.2. SLR flood simulations

Illustrations of GWI considering a 1-m SLR scenario are presented in figure 4. The hydrostatic method reproduces 65 percent (MSL) and 88 percent (MHHW) of the inundated area depicted by the 3D numerical method. In the MHHW case, 14 percent of the area inundated by the hydrostatic method lies outside of the 3D numerical-method inundation area. Thus, the total inundated area simulated using the hydrostatic method comes within 2 percent of the total inundated area simulated using the 3D numerical method. However, the flooded footprint of the two methods for the MHHW case differs by 26 percent as indicated by the uniquely flooded areas for the two methods (no overlap between two methods).

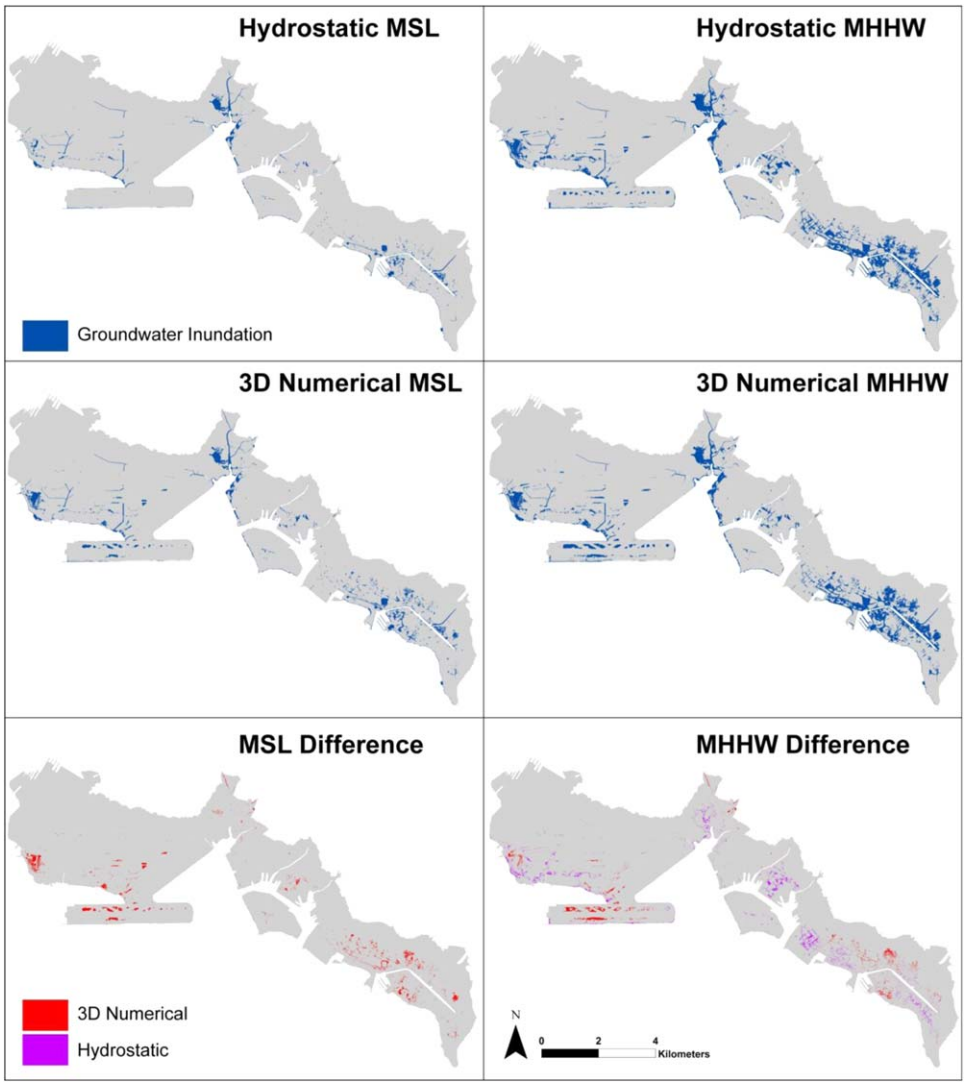

Figure 4. Simulations of 1 m SLR at MSL (left) and MHHW (right) showing GWI (blue). Top—Hydrostatic method. Middle—3D numerical method. Bottom—Uniquely flooded area (no overlap between two methods).

4. Discussion

As anticipated, our results reinforce 3D numerical modeling as the more robust of the two methods. Data assimilation by the 3D method provides for better representation of observed water levels. However, when referenced to MHHW, we find the hydrostatic approach produces simulations that are usefully accurate, with specific caveats.

Improved hydrostatic simulation of MHHW relative to MSL results from two offsetting and unrealistic assumptions inherent in the method. These are (1) that an aquifer has a hydraulic gradient equal to zero, and (2) that tidal signals do not attenuate as they move through an aquifer. These assumptions produce errors that are oppositely sensed. This explains why the hydrostatic method underestimates groundwater elevations (RMSE of 40 cm, Bias of -33 cm) in the MSL scenario, as only the negative bias of the first assumption is introduced. This results from the fact that in most areas in the MSL case the actual groundwater hydraulic gradient is oriented toward the coast.

Commonly used hydrostatic simulations conveniently and fortuitously are referenced to local MHHW (i.e., NOAA SLR Viewer). When referenced to MHHW, the hydrostatic method can produce reasonable estimations of groundwater elevation in low-lying coastal regions, especially given the limited effort required for model construction. Municipalities can employ the method as a first-cut approach towards revealing vulnerabilities to GWI.

However, the two methods produce localized differences in flood simulation (figure 4) that result from the ability of the 3D method to capture unique hydrological conditions (i.e., recharge, and conductivity) that influence tidal efficiency and head. These differences illustrate the inability of the hydrostatic method to produce

high-quality simulations that can be used as the basis for fine-scale decision making. Thus, we do not recommend use of the hydrostatic method alone for such endeavors. Rather, we advise it be used as an indicator of exposure to GWI at the municipal scale that could be used to inform decisions of whether methods of greater accuracy and precision are necessary. We recognize these findings apply specifically to the Honolulu area, since tidal ranges, topography, and hydraulic gradients vary regionally. However, because the minimum elevation of coastal groundwater generally exceeds that of local mean sea level in coastal regions (Turner *et al* 1997), it is reasonable to assume that where a coastal plain aquifer exists, the hydrostatic method (specifically considering a MSL tide stage) provides, at worst, a minimum estimate of groundwater elevation, and in turn GWI.

Use of the 3D numerical approach is more appropriate when (a) modeling coastal regions that feature particularly complicated conditions such as those that host extensive extraction/injection wells, (b) conducting modeling efforts that consider specific tidal scenarios (i.e. lower stages of the tide, extreme high tide); or (c) developing engineering techniques to mitigate flooding from GWI (i.e., implementation of extraction wells). We also note that, although the 3D numerical approach is more rigorous and widely applicable than the hydrostatic approach, the numerical approach may be unreliable if sufficient data are not available to constrain and evaluate model performance.

We also recognize that neither modeling approach presented here simulates dynamical coastal processes (i.e., coastal erosion, sediment accretion or changes in land cover (Lentz *et al* 2015, Anderson *et al* 2018)) that drive evolution of the landscape as sea level rises (FitzGerald *et al* 2008). Hence, our conclusions are most appropriately applied to regions, or environments that are less impacted by dynamical coastal processes (i.e. heavily developed shorelines that have been structurally hardened).

5. Summary and conclusion

Numerous coastal municipalities around the world face impacts from SLR flooding. The impacts are wide ranging and include disruptions in daily commerce, progressive failure of critical infrastructure, and intensified socio-economic burdens. In an effort to manage SLR impacts, informed, adaptive management is crucial and necessitates specific consideration of the various components of flooding including GWI. The GWI component is often overlooked in vulnerability studies, yet it is arguably the more challenging to manage as it includes complete saturation of the ground that is difficult to mitigate. This type of flooding can evade coastal armoring (i.e., seawalls, revetments, levees) and overwhelm traditional drainage conveyances, rendering them ineffective.

To spur consideration of GWI in policy and planning, a data-intensive 3D numerical method was developed by Habel *et al* (2017) to specifically simulate SLR induced GWI; however, its accessibility is limited by data requirements to produce robust simulations. Here we investigate applicability of the more simple and accessible hydrostatic method in simulating GWI. The hydrostatic method is commonly used to produce flood simulations considering a direct marine source; however its applicability towards simulating GWI had not previously been explored.

Comparison of the hydrostatic method to 3D numerical modeling reveals each method's ability to replicate present day groundwater levels at MSL and MHHW stages of the tide, and similarities of GWI simulations considering 1 m SLR. For Honolulu the hydrostatic method produces groundwater level and GWI simulations that are comparable to the more physically based method, specifically when referencing the local MHHW tide stage (generally typical of flood studies). Hydrostatic simulations produce a RMSE of 20 cm during the MHHW tide stage, compared to 10 cm produced by the 3D numerical method. Further, hydrostatic simulation of GWI in a scenario of 1 m SLR at MHHW reproduces 88% of the inundated area simulated using the 3D numerical method. However, because neither method has been designed to simulate dynamic landscape changes their use should be limited to settings or environments that are less impacted by dynamic coastal processes that accompany change as a result of SLR (i.e. regions that host widespread coastal armoring).

Though use of data-assimilating numerical modeling methods are more appropriate in cases where high accuracy simulations are necessary, we find that use of the hydrostatic method (specifically when referencing the local MHHW tide stage) is suitably accurate as a first-cut approach in identifying municipal vulnerabilities to GWI.

Acknowledgments

We gratefully acknowledge the Honolulu Board of Water Supply. Critical partnerships also included the Hawai'i State Department of Health, the U.S. Geological Survey, the Department of Land and Natural Resources, the Pacific Islands Climate Science Center, the H.K.L. Castle Foundation, the University of Hawai'i Sea Grant Program, the Honolulu Police Department, and the University of Hawai'i Coastal Geology Group. This study is sponsored by the Honolulu Board of Water Supply [Award Number C16545003] and partially supported by a grant/cooperative agreement from the National Oceanic and Atmospheric Administration, Project A/AS-1,

which is sponsored by the University of Hawaii Sea Grant College Program, SOEST, under Institutional Grant No. NA18OAR4170076 from NOAA Office of Sea Grant, Department of Commerce. The views expressed herein are those of the author(s) and do not necessarily reflect the views of NOAA or any of its subagencies. UNIHI-SEAGRANT-JC-18-09. This is SOEST contribution number 10706.

ORCID iDs

Shellie Habel https://orcid.org/0000-0001-9295-0596
Kolja Rotzoll https://orcid.org/0000-0002-5910-888X
Aly I El-Kadi https://orcid.org/0000-0002-9623-5458
Delwyn S Oki https://orcid.org/0000-0002-6913-8804

References

Anderson T R, Fletcher C H, Barbee M M, Romine B M, Lemmo S and Delevaux J M S M S 2018 Modeling multiple sea level rise stresses reveals up to twice the land at risk compared to strictly passive flooding methods *Sci. Rep.* **8** 14484

Bierbaum R, Smith J B, Lee A, Blair M, Carter L, Chapin F S III, Fleming P, Ruffo S, Stults M and McNeeley S 2013 A comprehensive review of climate adaptation in the United States: more than before, but less than needed *Mitig. Adapt. Strateg. Glob. Chang.* **18** 361–406

Bjerklie D M, Mullaney J R, Stone J R, Skinner B J and Ramlow M A 2012 Preliminary investigation of the effects of sea-level rise on groundwater levels in New Haven, connecticut *Open-File Report* 2012–1025 http://pubs.usgs.gov/of/2012/1025/

Church J A, Clark P U, Cazenave A, Gregory J M, Jevrejeva S, Levermann A, Merrifield M A, Milne G A, Nerem R S and Nunn P D 2013 *Sea level Change. Climate Change 2013: The Physical Science Basis. Contribution of Working Group I to the Fifth Assessment Report of the Intergovernmental Panel on Climate Change* (Cambridge, United Kingdom: Cambridge University Press)

Climate Ready Boston 2016 *Climate Ready Boston:* Final Report Online: https://boston.gov/sites/default/files/20161207_climate_ready_boston_digital2.pdf

Codiga D L 2011 Unified Tidal Analysis and Prediction Using the UTide Matlab Functions. Technical Report 2011-01

Cooper H M and Chen Q 2013 Incorporating uncertainty of future sea-level rise estimates into vulnerability assessment: a case study in Kahului *Maui Clim. Change* **121** 635–47

Cooper H M, Chen Q, Fletcher C H and Barbee M M 2013 Assessing vulnerability due to sea-level rise in Maui, Hawai'i using LiDAR remote sensing and GIS *Clim. Change* **116** 547–63

Cooper H M, Zhang C and Selch D 2015 Incorporating uncertainty of groundwater modeling in sea-level rise assessment: a case study in south Florida *Clim. Change* **129** 281–94

de Moel H, van Vliet M and Aerts J C J H 2014 Evaluating the effect of flood damage-reducing measures: a case study of the unembanked area of Rotterdam, the Netherlands *Reg. Environ. Chang.* **14** 895

Doherty J E and Hunt R J 2010 *Approaches to highly parameterized inversion—A guide to using PEST for groundwater-model calibration: U.S. Geological Survey Scientific Investigations Report 2010–5169*

Engott J A, Johnson A G, Bassiouni M, Izuka S K and Rotzoll K 2017 *Spatially Distributed Groundwater Recharge for 2010 Land Cover Estimated Using a Water-Budget Model for the Island of O'ahu, Hawai'i (ver 2., Dec 2017). Scientific Investigations Report 2015-5010* (Reston: US Geological Survey) (https://doi.org/10.3133/sir20155010)

Ferrall C C 1976 Subsurface geology of Waikiki, Moiliili and Kakaako with engineering application *Thesis for the degree of Master of Science* University of Hawaii at Manoa Geology and Geophysics; no.1397

Finstick S A 1996 Subsurface geology and hydrogeology of downtown Honolulu with engineering and environmental implications *ProQuest Dissertations Publishing* (Honolulu: Water Resources Research Center, University of Hawaii at Manoa) UMI Number: 9629823

FitzGerald D M, Fenster M S, Argow B A and Buynevich I V 2008 Coastal impacts due to sea-level rise *Annu. Rev. Earth Planet. Sci.* **36**

Gesch D B 2009 Analysis of lidar elevation data for improved identification and delineation of lands vulnerable to sea-level rise *J. Coast. Res.* 49–58

Gilmer B and Ferdaña Z 2012 *Developing a Framework for Assessing Coastal Vulnerability to Sea Level Rise in Southern New England, USA* (Dordrecht: Springer) pp 25–36

Gonneea M E, Mulligan A E and Charette M A 2013 Climate-driven sea level anomalies modulate coastal groundwater dynamics and discharge *Geophys. Res. Lett.* **40** 2701–6

Habel S, Fletcher C H, Rotzoll K and El-Kadi A I 2017 Development of a model to simulate groundwater inundation induced by sea-level rise and high tides in Honolulu, Hawaii *Water Res.* **114** 122–34

Hallegatte S, Green C, Nicholls R J and Corfee-Morlot J 2013 Future flood losses in major coastal cities *Nat. Clim. Chang.* **3** 802–6

Harbaugh A W 2005 *MODFLOW-2005, the US Geological Survey Modular Ground-water Model: the Ground-Water Flow Process* (Reston, United States of America: U.S. Geological Survey Techniques and Methods)

Hawai'i Climate Change Mitigation and Adaptation Commission 2017 *Hawai'i Sea Level Rise Vulnerability and Adaptation Report. Prepared by Tetra Tech, Inc. and the State of Hawai'i Department of Land and Natural Resources, Office of Conservation and Coastal Lands, under the State of Hawai'i Department of Land and Natural Resources Contract No: 64064*

Henman J and Poulter B 2008 Inundation of freshwater peatlands by sea level rise: uncertainty and potential carbon cycle feedbacks *J. Geophys. Res. Biogeosciences* **113**

Hinkel J, Lincke D, Vafeidis A T, Perrette M, Nicholls R J, Tol R S J, Marzeion B, Fettweis X, Ionescu C and Levermann A 2014 Coastal flood damage and adaptation costs under 21st century sea-level rise *Proc. Natl Acad. Sci.* **111** 3292–7

Horton R, Little C, Gornitz V, Bader D and Oppenheimer M 2015 New York city panel on climate change 2015 report chapter 2: sea level rise and coastal storms *Ann. N. Y. Acad. Sci.* **1336** 36–44

Izuka S K, Engott J A, Rotzoll K, Bassiouni M, Johnson A G, Miller L D and Mair A 2018 Volcanic aquifers of Hawai'i—Hydrogeology, water budgets, and conceptual models (ver. 2.0, March 2018): U.S. Geological Survey Scientific Investigations Report 2015-5164 (https://doi.org/10.3133/sir20155164)

Kane H H, Fletcher C H, Frazer N F and Barbee M M 2015 Critical elevation levels for flooding due to sea-level rise in Hawai'i *Reg. Environ. Chang.* **15** 1679

Kopp R E, Horton R M, Little C M, Mitrovica J X, Oppenheimer M, Rasmussen D J, Strauss B H and Tebaldi C 2014 Probabilistic 21st and 22nd century sea-level projections at a global network of tide-gauge sites *Earth's Futur.* **2** 383–406
Kopp R E, DeConto R M, Bader D A, Hay C C, Horton R M, Kulp S, Oppenheimer M, Pollard D and Strauss B H 2017 Evolving understanding of Antarctic ice-sheet physics and ambiguity in probabilistic sea-level projections *Earth's Futur* **5** 1217–33
Kopp R E, Hay C C, Little C M and Mitrovica J X 2015 Geographic variability of sea-level change *Curr. Clim. Chang. Reports* **1** 192–204
Kulp S and Strauss B H 2017 Rapid escalation of coastal flood exposure in US municipalities from sea level rise *Clim. Change* **142** 477–89
Lentz E E, Stippa S R, Thieler E R, Plant N G, Gesch D B and Horton R M 2015 Evaluating Coastal Landscape Response to Sea-Level Rise in the Northeastern United States-Approach and Methods *U.S. Geological Survey Open-File Report 2014–1252* (https://doi.org/10.3133/ofr20141252)
LiDAR Online 2017 Lidar Online: Worldwide LiDAR data and geoservices Online https://lidar-online.com/
Macdonald G A, Abbott A T and Peterson F L 1983 *Volcanoes in the Sea: the Geology of Hawaii* (Honolulu: University of Hawaii Press)
Marcy D *et al* 2011 New mapping tool and techniques for visualizing sea level rise and coastal flooding impacts *Solutions to Coastal Disasters 2011* (Reston, VA: American Society of Civil Engineers) pp 474–90
Mitchell M, Herschner C H, Herman J D, Schatt D E, Eggington E and Center for Coastal Resources Management, Virginia Institute of Marine Science 2013 Recurrent flooding study for Tidewater Virginia (Virginia: College of William and Mary) (https://doi.org/10.21220/V5TG79)
Munro K 1981 The subsurface geology of Pearl Harbor with engineering application *Thesis for the degree of Master of Science* University of Hawaii at Manoa Geology and Geophysicsno.1804
National Ecological Observatory Network (NEON) 2017 Open data to understand changing ecosystems Online http://neonscience.org/data/airborne-data
National Oceanic and Atmospheric Administration (NOAAa) 2017 Tide Station 1612340 Station Info Online: http://tidesandcurrents.noaa.gov/inventory.html?id=1612340
National Oceanic and Atmospheric Administration (NOAAb) 2017 Digital Coast Online https://coast.noaa.gov/digitalcoast/
National Oceanic and Atmospheric Administration (NOAAc) 2017 United States Interagency Elevation Inventory Online https://coast.noaa.gov/inventory/
Office of Resilience, Department of Regulatory and Economic Resources, Miami-Dade County, Florida 2016 *Assessment of Available Tools to Create a More Resilient Transportation System* Online: http://southeastfloridaclimatecompact.org/wp-content/uploads/2016/12/11.30.16-Final-Report-for-Assessment-of-Available-Tools-to-Create-a-More-Resilient-Transportation-System-Directive-160220.pdf
Oki D S 2005 Numerical simulation of the effects of low-permeability valley-fill barriers and the redistribution of ground-water withdrawals in the Pearl Harbor area *Oahu, Hawaii. Scientific Investigations Report* 2005–5253
OpenTopography 2017 OpenTopography: High-Resolution Topography Data and Tools Online http://opentopo.sdsc.edu/datasets
Office for Coastal Management 2019 Topographic Lidar DEM: Oahu from 2010-06-15 to 2010-08-15. NOAA National Centers for Environmental Information (https://inport.nmfs.noaa.gov/inport/item/52020)
Ponte R M 1994 Understanding the relation between wind-and pressure-driven sea level variability *J. Geophys. Res. Ocean* **99** 8033–9
Poulter B and Halpin P N 2008 Raster modelling of coastal flooding from sea-level rise *Int. J. Geogr. Inf. Sci.* **22** 167–82
Rotzoll K and El-Kadi A I 2007 *Numerical Ground-Water Flow Simulation for Red Hill Fuel Storage Facilities* (Oahu, Hawaii: NAVFAC Pacific) (ftp://ftp.soest.hawaii.edu/krotzoll/pub/ROTZOLL_%282007%29_RedHill_FlowModel.pdf)
Rotzoll K and El-Kadi A I 2008 Estimating hydraulic properties of coastal aquifers using wave setup *J. Hydrol.* **353** 201–13
Rotzoll K and Fletcher C H 2013 Assessment of groundwater inundation as a consequence of sea-level rise *Nat. Clim. Chang.* **3** 477–81
Rotzoll K, Oki D S and El-Kadi A I 2010 Changes of freshwater-lens thickness in basaltic island aquifers overlain by thick coastal sediments *Hydrogeol. J.* **18** 1425–36
Rutgers University NJADAPT 2017 Online http://njadapt.org/
Sherrod D R, Sinton J M, Watkins S E and Brunt K M 2007 *Geologic Map of the State of Hawai`i: U.S. Geological Survey Open-File Report 2007-1089* **1089** 1–83 (http://citeseerx.ist.psu.edu/viewdoc/download?doi=10.1.1.694.793&rep=rep1&type=pdf)
Spada G, Bamber J L and Hurkmans R 2013 The gravitationally consistent sea- level fingerprint of future terrestrial ice loss *Geophys. Res. Lett.* **40** 482–6
State of Hawaii Department of Health (DOH) 2018 Environmental Health Warehouse Online http://eha-web.doh.hawaii.gov/ehw/
Stearns H T and Vaksvik K N 1935 *Geology and Ground-Water Resources of the Island of Oahu* (Hawaii: Maui Publishing Company, Limited)
Strauss B H, Ziemlinski R, Weiss J L and Overpeck J T 2012 Tidally adjusted estimates of topographic vulnerability to sea level rise and flooding for the contiguous United States *Environ. Res. Lett.* **7** 14033
Sweet W V, Dusek G, Obeysekera J and Marra J J 2018 Patterns and projections of high tide flooding along the US coastline *NOAA Tech. Rep. NOS CO-OPS* **86** 1–56
Sweet W V, Kopp R E, Weaver C P, Obeysekera J, Horton R M, Thieler E R and Zervas C 2017 *Global and Regional Sea Level Rise Scenarios for the United States. NOAA Technical Report NOS CO -OPS 083* (Maryland: Silver Spring) Online https://tidesandcurrents.noaa.gov/publications/techrpt83_Global_and_Regional_SLR_Scenarios_for_the_US_final.pdf
Sweet W V and Park J 2014 From the extreme to the mean: Acceleration and tipping points of coastal inundation from sea level rise *Earth's Futur.* **2** 579–600
The New York State Sea Level Rise Task Force 2010 *New York State Sea Level Rise Task Force: Report to the Legislature* (New York) Online http://dec.ny.gov/docs/administration_pdf/slrtffinalrep.pdf
Turner I L, Coats B P and Acworth R I 1997 *Tides, waves and the super-elevation of groundwater at the coast J. Coast. Res.* **13** 46–60
US Army Corps of Engineers (USACE) National Coastal Mapping Program (NCMP) 2017 Joint Airborne Lidar Bathymetry Technical Center of Expertise Online http://shoals.sam.usace.army.mil/Mapping.aspx
United States Geological Survey (USGS) EarthExplorer 2017 Online https://earthexplorer.usgs.gov/
Whittier R B, Rotzoll K, Dhal S, El-Kadi A I, Ray C and Chang D 2010 Groundwater source assessment program for the state of Hawaii, USA: Methodology and example application *Hydrogeol. J.* **18** 711–23
Wu J, Zhang R and Yang J 1996 Analysis of rainfall-recharge relationships *J. Hydrol.* **177** 143–60
Yin B, Hou Y, Cheng M, Su J, Lin M, Li M and El-Sabh M I 2001 Numerical study of the influence of waves and tide-surge interaction on tide-surges in the Bohai Sea *Chinese J. Oceanol. Limnol.* **19** 97–102